High-Performance Pyroelectric Infrared Detectors

Marco Schossig, Volkmar Norkus, Gerald Gerlach

Technische Universität Dresden
Solid-State Electronics Laboratory
01062 Dresden
Germany

Abstract

We report on the fabrication of ultrathin self-supporting $LiTaO_3$ layers for high-performance pyroelectric single-element detectors. Thereby, only the area of the radiation-sensitive element is reduced to the desired thickness to keep the mechanical stability of the pyroelectric chip. This is done by an ion beam etching process at which a minimum thickness of 600 nm could be achieved. The small element thickness leads to a reduced heat capacity of the radiation-sensitive element resulting in a faster response. Time constants in the range of some milliseconds could be measured. Furthermore, the dielectric properties of the ultrathin lithium tantalate layers have been investigated. Measurements of the detector performance in vacuum revealed a maximum specific detectivity D^* of more than $5 \cdot 10^9$ cm $Hz^{1/2}$ W^{-1}.

Keywords: *pyroelectric infrared detector, thermal detector, high-detectivity infrared detector*

1 Introduction

Thermal infrared (IR) sensors like thin-film bolometers, thermopiles, and pyroelectric detectors are commonly used for monitoring IR radiation in the technically important wavelength range of 1…20 µm. During the last two decades, the usages of new materials and new technologies as well as the optimization of the sensor layout have lead to higher signal-to-noise ratio values of these IR detectors [1]. Most frequently used pyroelectric materials are triglycine sulfate (TGS) and its modifications [2], lithium niobate ($LiNbO_3$) [3], lithium tantalate ($LiTaO_3$) [3, 4], polymers (PVDF) [5, 6] and different kinds of ceramics (PZT, BST) [6]. Although detectors based on modified TGS have the highest signal-to-noise ratio a tremendous technological effort during crystal pulling and chip manufacturing is required. Therefore, the high cost of such detectors are only acceptable within the bounds of special use. However, for the fabrication of high-performance pyroelectric detectors the use of a material with a very low loss factor ($tan\ \delta$) is necessary. Here, pyroelectric detectors based on $LiTaO_3$ are most suitable because of their very low $tan\ \delta$ value of typically less than 0.001 (1 kHz, 25 °C) [7]. Moreover, they feature also a very low temperature dependency of the sensor parameters (responsivity R_V, specific detectivity D^*) as well as an excellent long-term stability and reproducibility of the detector characteristics.

The ultimately limiting performance of any thermal detector is set by the thermal fluctuation (TF) noise of the detector. For a detector at temperature T and in thermal equilibrium with an environment at the same temperature T, the minimum detectable power P_{min} (units of W) satisfies the equation [8]

$$P_{min} = \sqrt{4 \cdot k \cdot T^2 \cdot G \cdot \Delta f} \tag{1}$$

where k is the Boltzmann constant, G the thermal conductance (W/K) between the radiation-sensitive element and a heat sink, and Δf is the detection bandwidth in Hz. A very commonly used parameter for the comparison of a detector's performance is the area-normalized specific detectivity D^*

$$D^*_{TF} = \frac{\sqrt{A_D} \cdot \sqrt{\Delta f}}{P_{min}} = \sqrt{\frac{A_D}{4 \cdot k \cdot T^2 \cdot G}} \tag{2}$$

which is a measure for the signal-to-noise ratio. Here, A_D denotes the detector area. For a given operating temperature T, the maximum D^* occurs for the minimum G, which is set by radiation-coupling. For a radiation-coupled detector with unity emissivity ε, G is determined by thermal conductance G_{rad} via radiation [8, 9]

$$G_{rad} = 4 \cdot A_D \cdot \sigma \cdot T^3 \tag{3}$$

where σ is the Stefan-Boltzmann constant. Consequently, the radiation-coupled D^* satisfies the equation

$$D^*_{rad} = \sqrt{\frac{1}{16 \cdot k \cdot \sigma \cdot T^5}} \tag{4}$$

which is $1.8 \cdot 10^{10}$ cm $Hz^{1/2}$ W^{-1} for room temperature (T=300 K) and, therefore, denotes the theoretical maximum D^* value.

2 Detector design and fabrication process

Pyroelectric detectors based on $LiTaO_3$ are hybrid components. They consist of the pyroelectric chip with the responsive element and a preamplifier, which is at least a grounded-drain JFET. The two subcomponents are placed in a hermetic housing with an IR-transmissive window. Figure 1 shows the fundamental chip layout for high-performance single-element detectors.

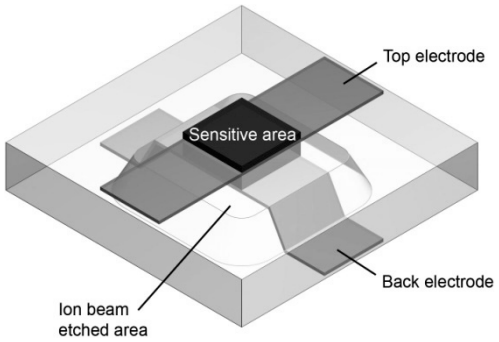

Fig. 1: Fundamental chip layout of a high-performance single-element detector with absorption layer and an ion beam etched cavity at the back side.

The mathematical-physical analysis of the signal and noise reactions shows that the thickness of the responsive element *d* at self-supporting chip arrangements has a fundamental influence on the signal-to-noise ratio of these IR detectors [10]. High signal-to-noise ratios can be achieved for this group of pyroelectric detectors by the use of particular thin responsive elements. The responsivity of the detector depends on the absorption coefficient α of the responsive element. For a metal-front-electrode / $LiTaO_3$ / metal-back-electrode set-up it amounts to approximately 0.6 in the wavelength range of (1…20) µm. It can be raised to more than 0.95 by applying special absorption layers, for instance metal black coatings [11, 12].

Figure 2 illustrates the manufacturing process of ultrathin self-supporting $LiTaO_3$ chips corresponding to Figure 1. The fabrication starts on polarized, monocrystalline $LiTaO_3$ wafers with a diameter of 2.5" and a thickness of about 500 µm. One side is polished and the other side is lapped. First, lift-off technique is applied to pattern the front electrode system photolithographically on the polished wafer side. The front electrode is made of $Ni_{80}Cr_{20}$ with a thickness of about 10 nm. A layer system of $Ni_{80}Cr_{20}$ and Au with a total thickness of about 50 nm is used to reinforce the front electrode outside the radiation-sensitive area. Afterwards, the polished side of the $LiTaO_3$ disc is cemented onto a circular blank with a maximum total thickness variation (TTV) of less than ± 1 µm. Mechanical and chemical-mechanical (CMP) polishing methods together with ion beam milling are used for thinning down the $LiTaO_3$. To etch the material locally in the radiation-sensitive area a photomask is applied. The thicker (≈ 20 µm) chip border area ensures the mechanical stability that is necessary for handling, in particular for assembly and bonding. In this way, the production of chips with responsive elements thinner than 2 µm are feasible. Thereby, the minimum usable thickness of the responsive element depends on the maximum TTV obtainable for crystal processing. Table 1 gives an overview of typical abrasion rates for the various subprocesses of the overall $LiTaO_3$ processing.

Table 1: Typical abrasion rates for the various subprocesses of the overall $LiTaO_3$ processing.

Process	Lapping	Polishing with diamond	Polishing with silica sol	Ion beam milling
Abrasion rate in nm/min	3,000…6,000	100…200	20…50	8…20

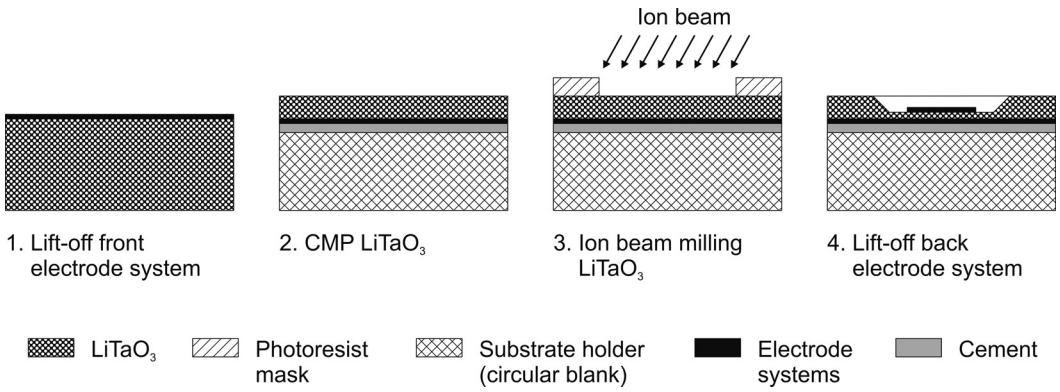

Fig. 2: Fabrication process for ultrathin self-supporting $LiTaO_3$ single-element detectors.

In this way, we were able to produce single-element detectors with a minimum element thickness of about 600 nm. The diameter of the ion beam etched area amounts up to 2.2 mm with a diameter of the sensitive area of 1 mm and 1.5 mm, respectively. The ultrathin $LiTaO_3$ chips are mechanically stable. The critical procedure is the lift-off of the back electrode system and the subsequent dissolution of the sensor chips from the blank. Once this is successfully done, the ultrathin $LiTaO_3$ chips can be handled like standard chips. The detector assembly as well as the bonding of the electrical contacts is easily manageable thanks to the thicker chip border area.

The total thickness variation that is usually obtained for crystal processing is shown in Fig. 3. Here, the best TTV is achieved within the chip center and is typically better than ± 0.5 µm over an area of (10x10) mm^2. Towards the chip corners the film thickness decreases rapidly. Therefore, ultrathin detector chips with comparatively large radiation-sensitive areas (typ. ≥ (1x1) mm^2) should be placed within the wafer center to obtain a homogeneous thickness distribution for the responsive element. In addition, the film thickness distribution of ultrathin (d < 0.8 µm) $LiTaO_3$ elements can be seen optically due to the appearance of interference fringes resulting from the interactions of the light reflections on front and back side. Here, broad and few interference fringes indicate a homogeneous element thickness. Fig. 4 shows an optical microscope image of an ultrathin $LiTaO_3$ sensor chip with a thickness of about 650 nm.

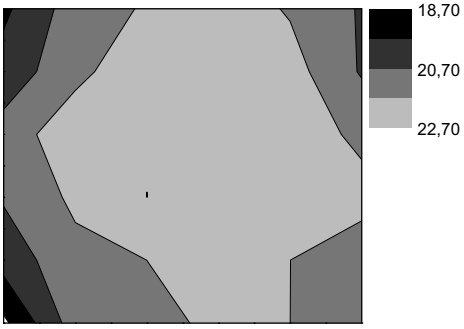

Fig. 3: Typical thickness distribution over the whole $LiTaO_3$ wafer (20x20 mm^2) after CMP crystal processing. Parameter: thickness d in µm.

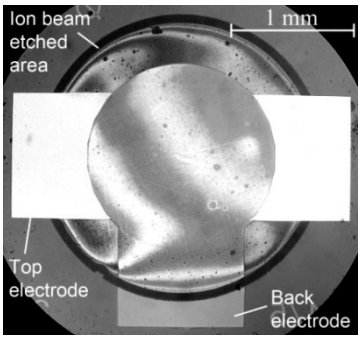

Fig. 4: Optical microscope image of an ultrathin $LiTaO_3$ chip. The interferences indicate the small element thickness of about 650 nm.

3 Dielectric properties

For sensors with a very high specific detectivity, noise due to the dielectric intrinsic loss tangent $tan\ \delta_i$ of the pyroelectric chip plays an important role [18]. It is caused by crystal defects or impurities. The higher the loss tangent is, the greater is the capacitor's equivalent series resistance to signal power. The lost energy is converted into heat resulting in a higher noise level and, therefore, in a worse signal-to-noise ratio. The entire measureable dielectric loss can be written as

$$tan\delta = tan\delta_T + tan\delta_i + tan\delta_R. \quad (5)$$

Advantageously, the dielectric intrinsic loss *tan* δ_i should be measured at around 1 kHz because here the other noise sources can be neglected. For $LiTaO_3$ bulk material *tan* δ_i amounts to approximately $1 \cdot 10^{-4}$ [13]. Within the frequency range of up to 100 Hz the influence of the thermal conditions cause an additional dielectric loss portion *tan* δ_T which exceeds the dielectric intrinsic loss *tan* δ_i [14]. At higher frequencies (≥ 10 kHz), an additional loss *tan* δ_R due to the contact resistance R_C becomes dominant which can be estimated by

$$tan\delta_R = \omega \cdot C_P \cdot R_C \tag{6}$$

where C_P is the capacitance of the responsive element and ω the angular frequency. Consequently, the influence of *tan* δ_R depends not only on the contact resistance but also on the element capacitance which, of course, increases with the reduction of the element thickness. For a capacitance of 635 pF (A_D = (1x1) mm^2, d = 0.6 µm), the contact resistance has to be smaller than 25 Ω to keep *tan* δ_R (1 kHz) ≤ 10^{-4}. This can be realized by an appropriate sample preparation so that *tan* δ_R can be neglected and the pure dielectric intrinsic loss *tan* δ_i can be measured at f = 1 kHz. Fig. 5 shows the measured loss tangent values for ultrathin $LiTaO_3$ layers. It can be seen that the dielectric intrinsic loss increases with reduced element thickness. This is caused by the increasing influence of imperfect surface layers which are a result of the crystal processing. Due to the mechanical thinning processes and the ion beam milling the crystal structure and/or composition is changed at the $LiTaO_3$ surface leading to imperfect surface layers. Therefore, the crystal processing has to be optimized to reduce the dielectric intrinsic loss of ultrathin $LiTaO_3$ elements.

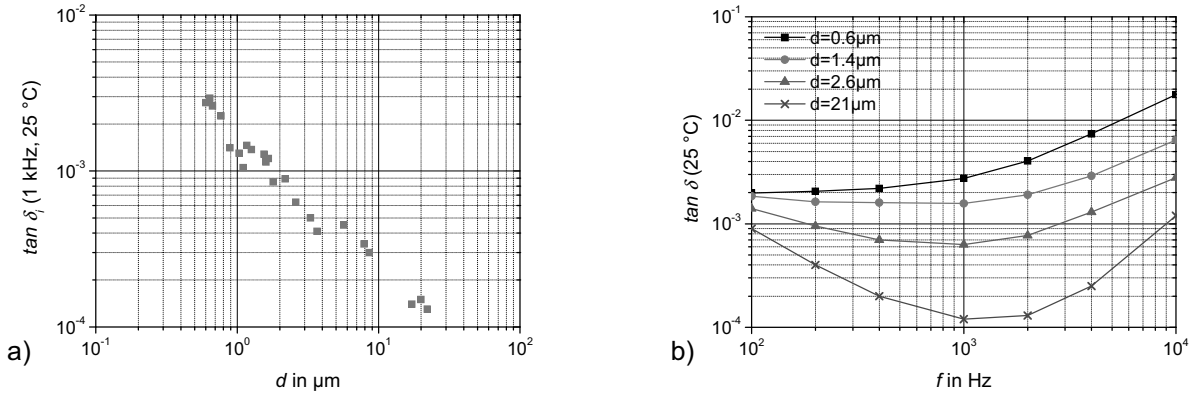

Fig. 5: Measured (a) dielectric intrinsic loss tangent versus element thickness and (b) total loss tangent versus frequency.

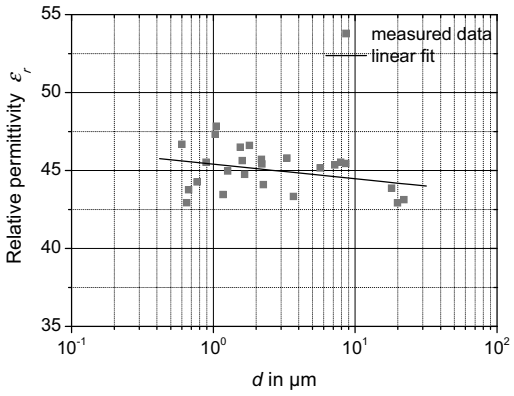

Fig. 6: Measured relative permittivity ε_r of ultrathin $LiTaO_3$ layers versus element thickness.

The relative permittivity ε_r of the ultrathin $LiTaO_3$ layers has been determined from the thickness and capacitance measurements regarding to

$$\varepsilon_r = \frac{C_P \cdot d}{\varepsilon_0 \cdot A_D} \tag{7}$$

where ε_0 is the vacuum permittivity. Fig. 6 shows the measured ε_r values in dependence on the element thickness. No significant influence could be observed. The measured values are within the bounds of the values (ε_r = 42.9...47) reported in literature [15-18]. Here, the exact measurement of the (medial) element thickness is difficult due to the non-uniform thickness distribution of the responsive element. This results in a broader distribution of the ε_r values for ultrathin $LiTaO_3$ elements. Apart from that, the linear fit of the measured data in Fig. 6 shows a slight increase of ε_r with reduced thickness. This is in good agreement with the numerical results of Chen et.al. [19] who had shown that imperfect surface layers increase the effective dielectric susceptibility and, hence, the relative permittivity at room temperature through lowering the phase transition temperature.

4 Measurement of the detector performance

The specific detectivity of pyroelectric sensors at low frequencies is mainly influenced by the thermal conditions within the sensor. For ultrathin $LiTaO_3$ layers, the heat conduction through the surrounding gas is the dominating heat exchange mechanism. Therefore, the evacuation of the detector housing is essential for high-performance pyroelectric detectors as it can be seen from Fig. 7. In addition, Fig. 8 shows the measured specific detectivity of ultrathin $LiTaO_3$ detectors with silver black coating. Here, an impressive value of D^*(500 K, 3 Hz) = $5.35 \cdot 10^9$ cm·Hz$^{1/2}$·W^{-1} could be obtained which is one third of the theoretical limit at room temperature and the highest value for $LiTaO_3$ detectors reported so far. The detectors are operated in voltage mode with a low-noise JFET and a high-ohmic resistor as preamplifier. The measurements were done with a black-body radiation source at T = 500 K and window transmission τ_w = 1. In the frequency range f = 10..300 Hz the *tan* δ noise is the dominating noise source and limits the detector performance. At lower frequencies, the preamplifier's current noise and at higher frequencies it's voltage noise exceed the *tan* δ noise.

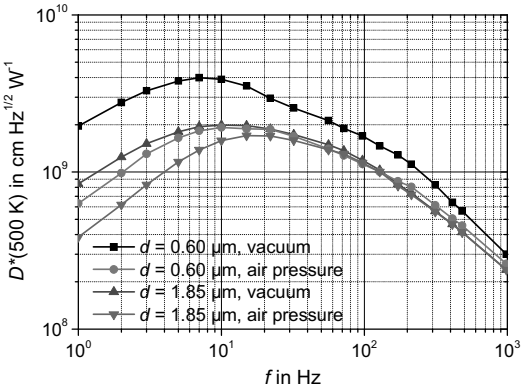

Fig. 7: Influence of vacuum on the specific detectivity D^* of ultrathin $LiTaO_3$ single-element detectors with A_D = 0.7854 mm^2.

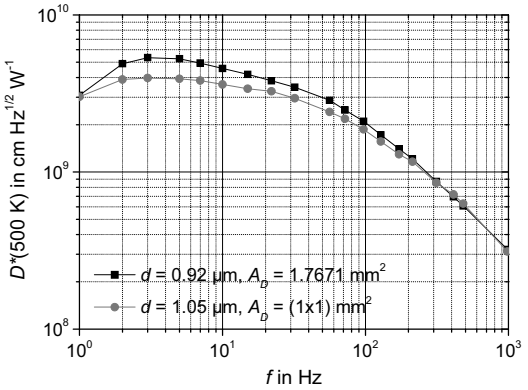

Fig. 8: Measured specific detectivity D^* of ultrathin $LiTaO_3$ single-element detectors with silver black coating in vacuum.

Table 2 summarizes the performance of the ultrathin $LiTaO_3$ single-element detectors. Here, thermal time constants in the range of some milliseconds could be measured. This is caused by the low film thickness leading to a reduced heat capacity of the responsive element and, therefore, to that fast response. The evacuation of the detector housing increased the thermal time constant by a factor of 2…3 depending on element thickness and detector area.

Table 2: Measured thermal time constants τ_{th} of various ultrathin $LiTaO_3$ single-element detectors.

Detector type	Thickness d in µm	Detector area A_D in mm^2	Thermal time constant τ_{th} in ms		D^*(500 K, 10 Hz) in cmHz$^{1/2}$W^{-1}
			air pressure	vacuum	
standard	20.9	0.7854	132	151	$2.32 \cdot 10^8$
standard	5.2	0.7854	76	136	$7.41 \cdot 10^8$
standard	1.85	0.7854	56	118	$1.99 \cdot 10^9$
standard	0.60	0.7854	17	53	$3.89 \cdot 10^9$
silver black	1.05	1 x 1	24	68	$3.61 \cdot 10^9$
silver black	0.92	1.7671	26	74	$4.56 \cdot 10^9$

5 Discussion

It was shown that the fabrication of ultrathin self-supporting $LiTaO_3$ layers with an element thickness $d < 1$ µm is feasible resulting in high-detectivity IR detectors. The detector performance is mainly influenced by the thermal conditions within the sensor. Thus, the evacuation of the detector housing is essential. In addition, the dielectric loss in ultrathin $LiTaO_3$ layers is increased due to imperfect surface layers resulting in a limitation of the detector performance within the frequency range in which pyroelectric detectors are normally operated. Finally, to achieve a performance close to the ideal background limit, the main requirements are: (1) further reduction of element thickness; (2) reduction of dielectric intrinsic loss; (3) better thermal isolation of the responsive element by a 3-dimensional patterning of the pyroelectric chip; (4) use of a very low-noise preamplifier; (5) application of an ultrathin absorption layer with very low thermal mass. The combination of these requirements will lead to uncooled thermal detectors with higher D^* values even closer to fundamental noise limits.

Acknowledgements

This work is part of the research program of the research training group “Nano- and biotechniques for the packaging of electronic devices” financially supported by the German Research Foundation (DFG).

References

[1] Rogalski A., “Infrared detectors: status and trends,” *Prog. Quantum Electron.* **27**, pp. 59-210, (2003).

[2] Neumann N., “Modified triglycine sulphate for pyroelectric infrared detectors,” *Ferroelectrics* **142**, pp. 83-92, (1993).

[3] Norkus V., Hofmann G., Möhling S., Budzier H., “Pyroelectric IR single-element detectors and arrays based on $LiNbO_3$ and $LiTaO_3$,” *SPIE* **1685**, pp. 155-163, (1992).

[4] Plehnert C., Norkus V., Möhling S., Hayes A., “Reactive ion beam etching of LiTaO3 and it’s application for pyroelectric infrared detectors,” *Surf. Coat. Technol.* **74-75**, pp. 932-936, (1995).

[5] Neumann N., Köhler R., Hofmann G., “Pyroelectric thin-film sensors and arrays based on P(VDF/TrFE),” *Integr. Ferroelectr.* **6**, pp. 213-230, (1995).

[6] Köhler R., Padmini P., Gerlach G., Hofmann G., Bruchhaus R., “Pyroelectric IR-detector arrays based on sputtered PZT and spin-coated P(VDF/TrFE) thin films,” *Integr. Ferroelectr.* **22**, pp. 383-392, (1998).

[7] Whatmore R. W., “Pyroelectric devices and materials,” *Rep. Prog. Phys.* **49**, pp. 1335-1386, (1986).

[8] Smith R. A., Jones F. E., Chasmar R. P., “The detection and measurement of infrared radiation,” Oxford University Press, Oxford, (1968).

[9] Hanson C. M., “Uncooled IR detector performance limits and barriers,” in *Proc. of SPIE AeroSense*, Vol. **4028**, Orlando, Florida, USA, 2000.

[10] Stokowski S. E., Venables I. D., Byer N. E., Ensign T. C., ”Ion-beam milled, high-detectivity pyroelectric detectors,” *Infrared Phys.* **16**, pp. 331-334, (1976).

[11] Hadni A., Gerbaux X., “Infrared and millimeter wave absorber structures for thermal detectors,” *Infrared Phys.* **30**, pp. 465-478, (1990).

[12] Lang W., Kuhl K., Sandmaier H., “Absorbing layers for thermal infrared detectors,” *Sens. Actuators*, A **34**, pp. 243-248, (1992).

[13] Stokowski S. E., “Temperature noise and dielectric loss in pyroelectric detectors,” *Appl. Phys. Lett.* **29**, pp. 393-395, (1976).

[14] Neumann N., Möhling S., “The influence of heat exchange between a sensitive element and its surroundings on the specific detectivity of pyroelectric detectors,” *Infrared Phys.* **34**, pp. 487-499, (1993).

[15] Fukuta K., Matsumura S., Yasuami S., Hirano H., Fukuda T., “$LiTaO_3$-substrate fabrication and characterization for pyroelectric sensors,“ *Jpn. J. Appl. Phys.* **20**, Suppl. 20-4, pp. 159-161, (1981)

[16] Smith R. T., Welsh F. S., ”Temperature dependence of the elastic, piezoelectric, and dielectric constants of $LiTaO_3$ and $LiNbO_3$,” *Appl. Phys. Lett.* **11**, pp. 2219-2230, (1971).

[17] Ping S. S., Lin L. H., “Dielectric and pyroelectric properties of $LiTaO_3$ single crystals,” *Ferroelectrics* **38**, pp.821-823, (1981).

[18] Putley E. H., “The possibility of background limited pyroelectric detectors,” *Infrared Phys.* **20**, pp. 149-156, (1980).

[19] Chen H., Lü T., Cao W., “Influence of imperfect surface layers on dielectric and pyroelectric properties of ferroelectric thin films,” *Physica B* **373**, pp. 177-181, (2006).